

## **Radiocarbon evidence for reduced deep water ventilation of the northern Indian Ocean during the last glacial maxima and early deglaciation**

**Kumari Nisha<sup>a,B</sup>, Sushant Suresh Naik<sup>a\*</sup>, Pankaj Kumar<sup>c</sup>, Barnita Banerjee<sup>d</sup> And P.B. Rama Murthy<sup>d</sup>**

<sup>a</sup>CSIR-National Institute of Oceanography, Dona-Paula, Goa 403004, India

<sup>b</sup>School of Earth, Ocean and Atmospheric Sciences, Goa University, Goa 403004, India

<sup>c</sup>Inter-University Accelerator Centre (IUAC), New Delhi, India

<sup>d</sup>CSIR-National Geophysical Research Institute, Hyderabad, India

Authors email: Kumari Nisha: nisha.121kumari@gmail.com

Nisha Kumari: ORCID: 0000-0001-7986-6015

\*Corresponding author E-mail: sushant@nio.org

### **Abstract**

Enhanced outgassing of sequestered carbon to the atmosphere by upwelling of deep water in the Southern Ocean during the last deglaciation is assumed to be the main factor that modulated changes in atmospheric CO<sub>2</sub> and atmospheric radiocarbon activity; however, the exact mechanism behind this deglacial CO<sub>2</sub> release still remains unclear. In this study, we have investigated ventilation changes in the deep waters of the northern Indian Ocean over the past 25 kyr BP using paired benthic and planktic foraminiferal radiocarbon, along with stable carbon and oxygen isotopes of benthic foraminifera, sedimentary CaCO<sub>3</sub>, content and coarse fraction from the gravity core SSD-044/GC-01(3160 m water depth) collected from Central Equatorial Indian Ocean. The results indicate greater proportion of southern sourced CO<sub>2</sub>-rich, poorly-ventilated Antarctic Bottom Water (AABW) during the Last Glacial Maximum (LGM) and Heinrich Stadial (HS1), in the northern Indian Ocean. The observed poor ventilation during the last glaciation show that the northern Indian Ocean was a part of the glacial ocean aged carbon pool. Improved ventilation during the Bølling-Allerød (B-A) is consistent with rapid resumption of Atlantic overturning circulation and inflow of North Atlantic Deep Water (NADW) into the northern Indian Ocean at the onset of the B-A, which caused flushing of the deep-carbon pool with evidence of degassing from the northern Indian Ocean. This study thus supports the role of Southern Ocean in modulating atmospheric CO<sub>2</sub> variations during the last deglaciation.

**Keywords:** radiocarbon, northern Indian Ocean, foraminifera, deglaciation, ventilation age, last glacial maximum.

## 1. Introduction

Deep-water being the largest reservoir of carbon at the Earth's surface, plays a very important role in modulating and regulating Earth's climate as it redistributes heat and influences the ocean-atmosphere CO<sub>2</sub> cycle (Sigman and Boyle, 2000). Deep waters formed at high latitudes of the North Atlantic, are then exported southwards where they mix and upwell in the Southern Ocean. The Southern Ocean is the region where deep water makes its first contact with the sea surface and the atmosphere (Primeau, 2005) and ventilates much of the respired carbon to the atmosphere. Hence, the Southern Ocean is considered to have played a crucial role in past atmospheric CO<sub>2</sub> fluctuations. It is known that during the northern hemispheric stadials: Heinrich Stadial 1 (HS1) and Younger Dryas (YD), there was an abrupt increase in atmospheric CO<sub>2</sub> (Monnin et al., 2001). Along with this increase in atmospheric CO<sub>2</sub>, there was a sudden drop in atmospheric radiocarbon activity ( $\Delta^{14}\text{C}$ ; Hughen et al., 2006; Reimer et al., 2020).

The mechanism for such atmospheric changes still remains uncertain. One of the possible sources for this drop in atmospheric  $\Delta^{14}\text{C}$  is assumed to be enhanced upwelling of <sup>14</sup>C depleted CO<sub>2</sub>-rich water from the Southern Ocean during the last deglaciation (Marchitto et al., 2007; Anderson et al., 2009; Skinner et al., 2010; Burke and Robinson, 2012; Skinner et al., 2015). According to this so-called 'Southern Ocean upwelling' hypothesis, during the last glaciation, the air-sea exchange in the Southern Ocean decreased due to factors like sea-ice cover (Stephens and Keeling, 2000), density stratification, and displacement of westerly winds (Toggweiler et al., 2006), which led to the isolation of deep water from the upper ocean and resulted in greater carbon storage in the glacial deep waters (Skinner et al., 2010; Burke and Robinson, 2012; Skinner et al., 2015; Ronge et al., 2016; Sikes et al., 2016). Continuous decay of radiocarbon due to restricted interaction with the atmosphere caused <sup>14</sup>C depletion in these isolated waters. Retreat of Antarctic sea-ice and southwardly shift of polar westerlies (Toggweiler et al., 2006) during the deglaciation led to enhanced upwelling of these old, carbon-rich deep waters and released the <sup>14</sup>C depleted CO<sub>2</sub> into the atmosphere (Anderson et al., 2009; Skinner et al., 2010).

One possible way of testing the 'Southern Ocean upwelling' hypothesis is to reconstruct past ocean ventilation changes, i.e. the rate at which atmosphere and oceanic interior exchange gases, which can be directly estimated from its radiocarbon content. The difference between the <sup>14</sup>C age of paired bottom-dwelling benthic and surface-dwelling planktic foraminifera provides the past changes in ventilation rate (Broecker et al., 1984; Broecker et al., 1990). It also indicates the extent of mixing of deep water with surface water. When there is lesser mixing between deep and surface water, the radiocarbon (and therefore CO<sub>2</sub>) exchange between these water masses also decreases, which will

result in a longer carbon sequestration time in the deep waters, making it radiocarbon depleted and hence the ventilation ages (the difference between  $^{14}\text{C}$  ages of benthic and planktic foraminifera) will be high, and vice versa. Similarly, the difference between the radiocarbon of deep water and the atmosphere provides an insight into carbon exchange between the atmosphere and the marine carbon pool. Thus, ventilation changes can be used as markers for past ocean circulation and climatic changes.

Numerous studies have been carried out in the Atlantic and Pacific Ocean, which investigated changes in intermediate and deep water radiocarbon content since the Last Glacial Maximum (LGM). Previous deep-water studies from the Atlantic and Pacific have suggested that glacial deep waters were  $^{14}\text{C}$  depleted (i.e. poorly ventilated) (Skinner and Shackleton, 2004; Galbraith et al., 2007; Barker et al., 2010; Burke and Robinson, 2012; Skinner et al., 2014). Studies from the intermediate water depths have shown an existence of poorly ventilated water mass in the Southern Ocean during the LGM, which was transported to the other oceans via the Antarctic Intermediate water mass (Marchitto et al., 2007; Bryan et al., 2010; Siani et al., 2013; Freeman et al., 2015; Ma et al., 2019). Such evidences from the Indian Ocean providing the Southern Ocean's role in atmospheric  $^{14}\text{CO}_2$  fluctuations are few. The Indian Ocean being solely ventilated from the south because of no deep-water formation, could be a suitable location to deduce the role of the Southern Ocean on past atmospheric  $\text{CO}_2$  variability.

There have been limited studies from the Indian Ocean that attempted to reconstruct the changes in radiocarbon distribution from intermediate waters (Bryan et al., 2010; Ma et al., 2019). These studies suggest the incursion of  $^{14}\text{C}$ -depleted Antarctic Intermediate Water (AAIW) in the Indian Ocean during the deglaciation (HS1 and YD). This  $^{14}\text{C}$  depletion in AAIW was because of mixing of old isolated abyssal water in south of the sub-Antarctic frontal zone. Interestingly, Naik et al., (2015) have reported outgassing of  $\text{CO}_2$  during the last deglaciation, possibly indicating release of sequestered carbon from intermediate water to the surface. Studies from the Indian sector of the Southern Ocean have shown that the Indian Ocean was part of a glacial aged carbon pool and suggested these  $^{14}\text{C}$  depleted,  $\text{CO}_2$ -rich waters from the southernmost Indian Ocean contributed to atmospheric  $\text{CO}_2$  rise during the deglaciation (Ronge et al., 2020; Gottschalk et al., 2020) albeit differing on the timing of  $\text{CO}_2$  release within the last deglaciation. . Though some studies have been carried out for deep water paleoceanographic changes in the northern Indian Ocean using stable isotope and geochemical tracers as a proxy (Kallel et al., 1988; Naqvi et al., 1994; Piotrowski et al., 2009; Ahmad et al., 2012; Singh et al., 2012; Chandana et al., 2017; Lathika et al., 2021; Bang et al., 2021), studies on radiocarbon changes in the deep water of Indian Ocean are limited (Naik and Nisha, 2020; Bharti et al., 2022). In this study, we have reconstructed ventilation changes in deep water of the northern Indian Ocean for the last 25 kyr using radiocarbon measurements from core SSD-044/GC-01. Results show evidence

for reduced ventilation in the Indian Ocean during the LGM and beginning of deglaciation (HS1) compared to the modern ocean and enhanced ventilation after ~14 kyr. Our results clearly support the role of the Southern Ocean in atmospheric CO<sub>2</sub> variation during the last deglaciation.

## **2. Material and methods**

### *2.1 Study Area*

The hydrography of the Indian Ocean is quite unique and different from the rest of the oceans. Surface hydrography is driven by the seasonal reversal of wind circulation during the monsoon. During summer monsoon (June-September) winds blow in the south-west (SW) direction whereas during winter monsoon winds blow in the north-east (NE) direction (Schott and McCreary, 2001). In response to wind, the surface water circulation also changes in the northern Indian Ocean. The surface water upto 150 m is comprised of a mixture of Arabian Sea High Saline Water (ASHSW) and low saline Bay of Bengal surface water. The intermediate depth of the northern Indian Ocean is occupied by northern sourced high saline Red Sea-Persian Gulf Water. Red Sea Water is found at depths of 600-800 m, whereas Persian Gulf Water is found at about 250-300 m. This northward flow of Red Sea-Persian Gulf Water is compensated by southern sourced AAIW, which is the dominant intermediate water mass in the Indian Ocean and is found up to 1500 m. Indian Indonesian Water from the Pacific Ocean enters the Indian Ocean at depths of 500-1500 m. Under modern conditions, deep water in the Indian Ocean is ventilated by southern sourced Circumpolar Deep Water (CDW), which is a mixture of well-ventilated, high-<sup>13</sup>C, nutrient-poor North Atlantic Deep Water (NADW), and poorly ventilated, CO<sub>2</sub> and nutrient-rich Antarctic Bottom Water (AABW) (You et al., 2000). The northward flowing CDW after entering the Indian Ocean flows through three different paths; western pathway - Deep Western Boundary Current (DWBC), the central pathway, and one along the ninety-east ridge (Piotrowski et al., 2009). The Upper Circumpolar Deep Water (UCDW) is mainly composed of NADW and a lesser fraction of AABW. It flows between a water depth of 2-3.8 km. Below 3.8 km is the Lower Circumpolar Deep Water (LCDW), which has AABW as a major component and a small proportion of NADW.

The gravity core SSD-044/GC-01 was raised from a water depth of 3160 m during the RV Sindhu Sadhana cruise No. 44 from the northern Indian Ocean (4.99° N; 76.99° E) (Fig. 1a and b), within the Central Indian Basin. At present, the core is ventilated by a water mass primarily sourced from the northward circulating UCDW, which has a greater component of NADW (Piotrowski et al., 2009). The region is affected by the seasonal reversal of boundary currents. The sediment core was subsampled at 1 cm interval to a length of 100 cm. The samples were oven dried for 24 hrs at a temperature

of 50-60° C. The weight of the dried samples was measured and then were soaked for 24 hrs in 100 mL distilled water for the samples to disintegrate. The disintegrated samples were wet sieved through a 63 µm mesh in order to remove clay particles. Washing of the samples was done carefully to avoid breakage of foraminifera. The retained coarse fraction (>63 µm) was collected in a beaker and kept in an oven at 60° C for drying. The dried coarse fraction was then collected in 10 mL vials.

## 2.2 Radiocarbon measurements for age model and ventilation ages

Radiocarbon dates were obtained using paired samples of mixed-species of benthic foraminifera (excluding pyrgo and agglutinated species), and mono-species planktic foraminifera (*Globigerinoides ruber*). In a few cases of planktic foraminifera *Globigerinoides quadrilobatus* was also picked to obtain the required weight for AMS analysis (~13 mg). For radiocarbon measurement, a representative aliquot of the coarse fraction was dry-sieved through a >250 µm sieve, from which paired intact benthic and planktic foraminifera were handpicked using a stereozoom microscope, and wherever the picked sample weight was < 13 mg, foraminifera from size fraction 150-250 µm were also picked. For some benthic samples, specimens from two adjoining intervals were combined to attain the sufficient weight for AMS dating. AMS <sup>14</sup>C dates were measured at the Inter-University Accelerator Centre (IUAC), New-Delhi, India. Radiocarbon ages for the core SSD-044/GC-01 are summarized in supplementary data (Table 1 and 2, supplementary material; Fig. 2a). Here the ventilation ages of deep water are reported as radiocarbon age which is the difference between paired bottom-dwelling benthic foraminifera and surface-dwelling planktic foraminifera (B-P) based on Broecker et al., (1984) which represents sub-surface radiocarbon age offset.

## 2.3 Age Model

The age model for the top 100 cm of the core was established from the AMS <sup>14</sup>C dates derived from planktonic foraminifera from a size fraction of >250 µm (Table 1, supplementary material) We have used an age-depth modelling routine named *Undatable*, which is developed in MATLAB and uses Bayesian radiocarbon (<sup>14</sup>C) calibration software (MatCal) (Lougheed and Obrochta, 2019). These <sup>14</sup>C ages based age models were calibrated using IntCal20 calibration data. Downcore median ages, confidence intervals, and a density cloud that displays the most likely regions of age-depth probability were calculated by linearly interpolating all *nsim* number of unique age-depth (Lougheed and Obrochta, 2019) runs to 1 depth unit resolution (e.g., cm), and then computing the 1st to 99th percentiles of the ages corresponding to each depth unit. Darker regions of the density cloud are closer to the 50th percentile (Fig. 2b). A reservoir correction of  $\Delta R = -91 \pm 25$  years was used (Dutta et al., 2001; Southon et al., 2002). A few of the AMS <sup>14</sup>C dates were adopted from Yadav *et. al.*, (2021), and

re-calibrated using the above procedure. The average sedimentation rate of the core is ~3.5 cm/year (Fig. 2c)

#### 2.4 Total Inorganic Carbon (TIC)

Total Inorganic Carbon analysis was done on 10-12 mg of finely ground sediment samples using UIC CM5015 Coulometer. The values are reported as percentage of CaCO<sub>3</sub>. Replicate analysis on ten samples yielded a repeatability of ±2 %.

#### 2.5 Stable Carbon and Oxygen Isotope

Stable carbon and oxygen isotopes were generated using epifaunal benthic foraminifera *Cibicidoides wuellerstorfi*. For each interval, 3-5 well-preserved foraminifera (>250 μm), with no apparent dissolution, were picked. Isotopic measurement was performed on a Thermo Finnigan Gas Bench II, equipped with a CTC auto-sampler and coupled to a Delta Plus XP Mass Spectrometer with a precision better than ±0.06 ‰ for δ<sup>13</sup>C and ±0.08 ‰ δ<sup>18</sup>O. Calibration was carried out against V-PDB (Vienna Pee Dee Belemnite) standard using an in-house dolomite standard subsequent to linearity correction that has been calibrated against NBS-18 and NBS-19 reference standards.

#### 2.6 Coarse Fraction

The coarse fraction content in all the samples was calculated as the weight of the dried coarse fraction (>63 μm) divided by the total weight of the dry sediment multiplied by hundred.

### 3. Results

The reconstructed benthic-planktic (B-P) ventilation ages for deep waters suggest that there have been significant changes in deep-water ventilation during the last 25 kyr (Fig. 3a). The apparent age difference between coexisting benthic and planktic foraminifera was ~2500 to 3000 <sup>14</sup>C years during the LGM (~24 -17.5 kyr BP) indicating poorly ventilated water at the core location. The ventilation age remained high during the HS1 (~17.5-14.5 kyr BP) and was around 3000 <sup>14</sup>C years, indicating lowered radiocarbon activity of deep water. At the start of the Bølling-Allerød (B-A; ~14.5-12.8 kyr BP), there was an abrupt reversal in the ventilation age of deep water. The ventilation age significantly decreased to as low as ~1500 <sup>14</sup>C years indicating better ventilated deep water at that time. During the YD (~12.8-11.5 kyr BP) there was a small increase of ~300 <sup>14</sup>C years in the ventilation age, which further showed a decrease during the Holocene and was ~1500 <sup>14</sup>C years, indicating relatively better ventilation of water.

Calcium carbonate content of sediment complements the radiocarbon data (Fig. 3b). In glacial sediments, the average CaCO<sub>3</sub> was ~53 %, showing lower values at the beginning of LGM and an

increase towards the end of it. At the beginning of deglaciation, CaCO<sub>3</sub> began to decline, reducing to ~54 % during the HS1. During the B-A, there was a sudden increase in CaCO<sub>3</sub> content, which further reached up to ~62 % at ~ 12 kyr BP. Thereafter CaCO<sub>3</sub> content declined into the Holocene with an increase during the late Holocene.

Stable carbon isotopic ( $\delta^{13}\text{C}$ ) records of benthic foraminifera *Cibicidoides wuellerstorfi* showed an increasing trend from the LGM to the Holocene (Fig. 3c). Stable carbon isotopic values range from -0.6 ‰ to 0.4 ‰ for the last 25 kyr BP. The  $\delta^{13}\text{C}$  values remained low at ~ -0.4 ‰ during the LGM and HS1. There was a gradual rise in  $\delta^{13}\text{C}$  values through the B-A and YD. This was followed by a short drop and then an increase during the Holocene with values reaching up to ~0.4‰ at 4 kyr BP, followed by a slight drop in the late Holocene. The oxygen isotopic ( $\delta^{18}\text{O}$ ) values showed a decreasing trend from the LGM to the Holocene (Fig. 3d). The  $\delta^{18}\text{O}$  values fluctuated between 4.4 ‰ and 2.6 ‰ for the last 25 kyr BP. Maximum  $\delta^{18}\text{O}$  values were recorded during LGM and HS1. The  $\delta^{18}\text{O}$  values decreased at the B-A, decreased further at the YD and then gradually decreased through the Holocene.

The percentage of CF ranged from ~12- 24% (Fig. 3e). The major component of the coarse fraction was biogenous remains with almost no lithogenous fraction for the last 25 kyr BP. The CF % was low during the LGM and HS1. Coarse fraction started to increase from the B-A into the YD, and showed a gradual decrease during the Holocene.

## 4. Discussion

### 4.1 Deep water ventilation changes in the northern Indian Ocean

Reconstruction of deep water <sup>14</sup>C ventilation age along with benthic stable carbon and oxygen isotope, CaCO<sub>3</sub>, and coarse fraction data from the core SSD-044/GC-01 imply changes in deep water ventilation/source for the last 25 kyr. The difference between benthic- planktic <sup>14</sup>C age was higher (~2500-3000 <sup>14</sup>C years) during the LGM than in the modern ocean (Fig. 3a). These high ventilation ages during the LGM indicate a strong stratification between the upper and deep water masses and hence poor ventilation existing during that time. We suspect that this poorly ventilated water at our core site originated from a glacially isolated deep-water mass. Studies from the Indian Ocean have suggested that during the LGM, the export of northern sourced water into the Indian Ocean was reduced and was compensated by an increased flow of southern sourced water (Curry et al., 1988). Neodymium (Nd) isotope and ventilation age records of deep water masses in the northern Indian Ocean have also shown a reduced flow of NADW and an increased penetration of nutrient and CO<sub>2</sub>-rich southern sourced water during the LGM (Piotrowski et al., 2009; Lathika 2021; Bang et al., 2021; Bharti et al., 2022). Results from a modelling study suggests the LGM ocean circulation state was

characterized by a weak (10–15 Sv) and relatively shallow (2000–2500 m) NADW cell, and a reduced AABW transport (Menviel et al., 2017). A weaker AABW formation rate at the LGM could result from the presence of grounded ice over today's main AABW formation regions such as the Ross and Weddell Seas, and/or weakened or equatorward shifted Southern Hemispheric Westerlies (Menviel et al., 2017). The overall reduced oceanic ventilation at the LGM thus enhanced the efficiency of the oceanic biological pump by enhancing the storage of respired carbon in the ocean interior without causing anoxia (Galbraith and Jaccard, 2015; Menviel et al., 2017). Therefore, reduced deep ocean ventilation during the glaciation would contribute to lowering atmospheric CO<sub>2</sub>, with important implications for past carbon cycle and climate changes (Skinner et al., 2017). Zhang et al., 2022 state that the persistent northward inflow of CDW with corrosive Pacific waters contribution must have been responsible for the ventilation of the deep Indian Ocean during the glacial. Thus majority studies infer presence of CO<sub>2</sub>-rich, poorly-ventilated deep-water mass during the glacial, which probably filled the deeper parts of the Indian Ocean.

Variations in CaCO<sub>3</sub> content complement our radiocarbon data (Fig. 3b). Low values of CaCO<sub>3</sub> are recorded during the LGM, which could either be because of low surface productivity, dilution by terrigenous influx, or dissolution at the sea floor. Yadav et al., (2021) have reported high surface productivity during the LGM from the same core, and hence low CaCO<sub>3</sub> content at the core site is not driven by productivity. Dilution can be a factor for this low CaCO<sub>3</sub>, but the low sedimentation rate during the LGM does not support dilution as an important factor (Fig. 2c). Calcium carbonate data is consistent with the coarse fraction record from the same core (Fig. 3e). Low coarse fraction along with low CaCO<sub>3</sub> during the LGM indicates decreased preservation and increased dissolution, implying low bottom-water CO<sub>3</sub><sup>2-</sup> concentration and hence CO<sub>2</sub> enriched water prevailing at that time. Thus high ventilation age and low CaCO<sub>3</sub> suggest less-ventilated (as compared to the modern ocean), CO<sub>2</sub>-rich glacial water prevailed in the northern Indian Ocean.

The δ<sup>13</sup>C values of benthic foraminifera can be used as a tracer of deep water circulation, complementary to <sup>14</sup>C ventilation ages. Benthic foraminifer's carbon isotopic records from the northern Indian Ocean have shown significant changes in deep water chemical characteristics since the last glaciation (Kallel et al., 1988; Ahmad et al., 2012). During the LGM, low δ<sup>13</sup>C values of ~ -0.4 ‰ were recorded in our core (Fig. 3c), indicating incursion of nutrient-rich and poorly ventilated water. This low δ<sup>13</sup>C is consistent with previously published records from the northern Indian Ocean which have been interpreted as reduced export of NADW, which was compensated by increased export of nutrient-rich southern sourced water in the Indian Ocean (Duplessy et al., 1984; Naqvi et al., 1994; Ahmad et al., 2012; Raza et al., 2014). The glacial-interglacial δ<sup>18</sup>O shift of ~ 1.4 ‰ (difference



between the  $\delta^{18}\text{O}$  average of LGM and early Holocene) exceeds the ice volume change by 0.4 ‰, which indicates cooler deep waters during the LGM (Fig. 3d). Hence, high  $\delta^{18}\text{O}$  values during the LGM can be linked to an increased inflow of cold southern sourced deep water masses into the northern Indian Ocean. Thus lowered  $\delta^{13}\text{C}$  and high  $\delta^{18}\text{O}$  support the reduced flow of northern-sourced deep waters, countervailed by glacial-aged southern sourced  $^{14}\text{C}$  depleted waters at the core site. There is also a mismatch between the trend in ventilation ages and  $\delta^{13}\text{C}$ , at  $\sim 20$  kyr (Fig. 3a and c). Though we see a drop in ventilation age of  $\sim 500$  yrs, the  $\delta^{13}\text{C}$  remain almost unchanged. This could occur due to increasing air-sea disequilibrium of carbon isotopes with lowered  $p\text{CO}_2$ . Under low atmospheric  $p\text{CO}_2$  conditions of the glacials,  $\Delta^{14}\text{C}$  is known to increase, and surface reservoir age to increase by  $\sim 250$  yrs throughout the world ocean (Galbraith et al., 2015).

Poorer ventilation (high ventilation ages) of deep waters during the last glaciation in comparison to the modern, has been noted by other studies in the Indian Ocean (Gottschalk et al., 2020; Bharti et al., 2022), the Atlantic (Barker et al., 2010; Skinner et al., 2010) and Pacific Ocean (Galbraith et al., 2007; Rafter et al., 2022). High ventilation ages of the Indian Ocean along with the records from the other oceans suggest significant aging of Southern Ocean deep water (hence,  $^{14}\text{C}$  depleted) during the glacial time. This  $^{14}\text{C}$  depletion could be possibly the result of a decrease in the exchange of gases between the atmosphere and deep water during the LGM which led to continuous decay of  $^{14}\text{C}$  (Skinner et al., 2010).

Similar to the LGM, deep-water ventilation in the northern Indian Ocean during the HS1 remained poor (Fig. 3a). This period is associated with the melting of icebergs in the North Atlantic. Massive discharge of glacial ice and more freshwater input led to the reduced formation and shoaling of the NADW and hence resulted in the weakening of AMOC at this time (Elliot et al., 2002; McManus et al., 2004). These changes in the production of NADW led to decreased export of NADW into the Atlantic (Skinner and Shackleton, 2004; Freeman et al., 2015) and Pacific Ocean (Galbraith et al., 2007). In the Indian Ocean, stable isotopic and geochemical studies suggest a decrease in the export of northern sourced water (Piotrowski et al., 2009; Ahmad et al., 2012; Bharti et al., 2022). Intermediate water studies from the Indian Ocean have pointed to an increased export of southern sourced water into the Indian Ocean (Jung et al., 2009; Ma et al., 2019; Ma et al., 2020). Direct evidence of increased penetration of southern sourced AAIW due to reduced inflow of northern sourced water have been reported using  $^{14}\text{C}$  (Bryan et al., 2010) and  $\epsilon_{\text{Nd}}$  (Yu et al., 2018) proxies. Therefore, the increased ventilation ages at our core site during the HS1 suggests a reduced export of NADW into the northern Indian Ocean. This strongly suggests a greater proportion of southern sourced

poorly ventilated AABW inflow as a result of NADW shoaling. The high ventilation ages are very well correlated with  $\text{CaCO}_3$  and  $\delta^{13}\text{C}$  values.

Studies from the Atlantic Ocean (Skinner and Shackleton, 2004; Robinson et al., 2005; Barker et al., 2010; Skinner et al., 2010) and Pacific Ocean (Galbraith et al., 2007; Marchitto et al., 2007) have reflected increased penetration of NADW during the B-A, since the resumption of AMOC led to extensive formation of NADW at this time (McManus et al., 2004; Böhm et al., 2015). Stable isotope data from the Indian Ocean have also shown an increase in northerly sourced better ventilated water during the B-A (Ahmad et al., 2012, Raza et al., 2014; Ma et al., 2019). In addition, Nd isotopic record points to an expansion of the NADW in the Indian Ocean (Piotrowski et al., 2009). In our study, the HS1 was followed by an abrupt decrease in deep water ventilation age (better ventilation) during the B-A (Fig. 3a), suggesting a major shift in deep water circulation. We suspect that this low ventilation age could be the result of intensified penetration of better ventilated northern sourced deep water at the core site. A shift in  $\text{CaCO}_3$  to higher values was observed in the B-A with a peak in the YD, indicating better preservation of  $\text{CaCO}_3$  suggests incursion of better ventilated water during this period (Fig. 3b). This is also supported by an increase in coarse fraction % beginning from the B-A (Fig. 3e). A marked positive shift in  $\delta^{13}\text{C}$  from B-A onwards, indicates a progressive influx of nutrient-depleted and better ventilated NADW at the core site.

This increase in ventilation was followed by a short-term reduction in deep water ventilation during the YD. The ventilation age increased by  $\sim 300$   $^{14}\text{C}$  years during this cold stadial. This time coincides with the partial weakening of the AMOC (McManus et al., 2004). The reduction in NADW formation was less intense compared to that during the HS1, which is why the decrease in ventilation during YD was less pronounced than HS1 at the core site. Low ventilation age along with high  $\text{CaCO}_3$  and  $\delta^{13}\text{C}$  during the Holocene indicate that the deep waters were well ventilated as compared to the LGM. Combined results of ventilation age,  $\text{CaCO}_3$ ,  $\delta^{13}\text{C}$  and  $\delta^{18}\text{O}$  data suggest an increased export of NADW during the Holocene and less dominance of southern sourced deep water in the UCDW.

#### *4.2 Redistribution of $^{14}\text{C}$ depleted water from the Southern Ocean*

The benthic-planktic ventilation age variations seen in the Indian Oceans studies; cores SSD-044/GC-01 (this study), RC27-23 (Bryan et al., 2010), SS152/3828 and SS172/4040 (Bharti et al., 2022) are consistent with the increase in atmospheric  $\text{CO}_2$  and atmospheric  $\Delta^{14}\text{C}$  decline during the deglaciation (Fig. 4). Atmospheric  $\text{CO}_2$  rose in two steps during the deglaciation, during the HS1 and the YD (Monnin et al., 2001). Rising deglacial atmospheric  $\text{CO}_2$  levels are related to the upwelling of deep,  $\text{CO}_2$ -rich water masses to the surface of the Southern Ocean (Broecker and Barker, 2007; Anderson et

al., 2009). Vertical mixing in the Southern Ocean is a result of interference of Antarctic Circumpolar Current (ACC) with local bathymetry. At the onset of HS1, deep-ocean  $^{14}\text{C}$  ventilation increased until 16.3 kyr BP, signaling a net loss of remineralized carbon from the deep ocean during that time interval as a result of reinvigorated vertical mixing (Core MD12-3396CQ; Gottschalk et al., 2020 and references therein). However, our core record does not have sufficient number of data points during the LGM and early HS1 to understand if the Southern Ocean signal was transmitted into the northern Indian Ocean. Later to ~16.3 kyr BP, ventilation age records from south of  $40^\circ$  S show a return to glacial-like condition, which relates to a ventilation decrease, a unique feature of the deep South Indian Ocean due to inter-basin differences (Gottschalk et al., 2020). Our ventilation ages are highest at ~3000 years during the HS1. This inter-basin heterogeneity abruptly dissipated at the end of HS1, when the ventilation age and oxygen characteristics of deep waters in the different ocean basins rapidly approached prebomb values for the first time throughout the deglaciation (Gottschalk et al., 2020). We find a sharp decrease in ventilation ages beginning at ~ 14.6 kyr as observed in the Southern Indian Ocean core MD12-3396CQ and deep-sea corals from the Drake Passage (Southern Ocean; Burke and Robinson, 2012). The fast increase in  $^{14}\text{C}$  and  $\text{O}_2$  ventilation in the South Indian Ocean at the end of HS1, at ~14.6 kyr BP, is linked to a rapid resumption of Atlantic overturning at the onset of the B-A warm period, which caused homogenization of the entire South Indian water column, laterally and vertically (Gottschalk et al., 2020). The ventilation age records from the northern Indian Ocean along with atmospheric  $\Delta^{14}\text{C}$  (Reimer et al., 2020) relate well to the Southern Ocean upwelling indices (Fig. 4d) pointing towards the Southern Ocean as the source for redistribution of aged carbon to the other oceans, and to the atmosphere (Anderson et al., 2009).

During the YD, we find a slight increase in ventilation age (poorer ventilation) in core SSD-044/GC-01 (Fig. 3a). In line with our observation, the South Indian Ocean was a moderate source of carbon to the atmosphere during the YD and did not significantly contribute to the late deglacial  $\text{CO}_{2,\text{atm}}$  increase (Gottschalk et al., 2020). At the end of YD, however, there was a rapid loss of carbon from the South Indian Ocean mediated by stronger Atlantic overturning and wind-driven Ekman pumping (Gottschalk et al., 2020). These authors call attention to spatial differences in timing of  $\text{CO}_2$  release from the Southern Ocean, possibly due to lateral variations in the mode and rate of AABW formation and/or the efficiency of air-sea gas equilibration. Coinciding with the low ventilation ages in the deep waters of the Southern Ocean, aged  $^{14}\text{C}$  has been observed in the intermediate waters of the western Arabian Sea during the HS1 and YD (Bryan et al., 2010; Fig. 4c). The explanation provided was the release of  $^{14}\text{C}$ -depleted carbon from the deep ocean by renewal of upwelling and mixing in the Southern Ocean and further incorporation into thermocline and intermediate water masses of the Southern Ocean, and

spread northward into the Pacific, Indian and Atlantic Ocean basins (Bryan et al., 2010). However, an outgassing of CO<sub>2</sub> at ~14.4-14.2 kyr concomitant to the CO<sub>2</sub> increase of 12 ± 1 ppm of the atmosphere has been reported from the surface water of the eastern Arabian Sea, which was reasoned to be indicative of the upwelling of a nutrient-enriched water mass of Southern Ocean origin (Naik et al., 2015; Fig. 4e). This observation of CO<sub>2</sub> outgassing during the B-A is in agreement with the increase in <sup>14</sup>C and O<sub>2</sub> ventilation in the South Indian Ocean linked to a rapid resumption of Atlantic overturning (Gottschalk et al., 2020). The possible link between near-identical timing of CO<sub>2</sub> outgassing from the eastern Arabian Sea during the B-A, the improved ventilation of deep-waters of the northern Indian Ocean during the B-A (present study), and the increase in <sup>14</sup>C and O<sub>2</sub> ventilation in the South Indian Ocean seems to be the flushing of the deep-ocean carbon pool, not only limited to the Southern Ocean, but with a wider impact, in the northern Indian Ocean. Hence our data supports the hypothesis that the Southern Ocean upwelling had a vital role in atmospheric CO<sub>2</sub> variation during the deglaciation (Anderson et al., 2009; Skinner et al., 2010). Furthermore, our data suggests that the northern Indian Ocean could have also contributed to the atmospheric CO<sub>2</sub> rise during the deglaciation (specifically the B-A).

## 5. Conclusions

The ventilation data from core SSD-044/GC-01 illustrates changes in northern Indian Ocean deep water circulation and its relation to climatic changes across the last 25 kyr. The results indicate that during the LGM and the HS1, poorly-ventilated CO<sub>2</sub>-rich glacial water prevailed in the northern Indian Ocean. This suggests a greater proportion of southern sourced poorly ventilated AABW filled up majority of the oceans, which could be due to shoaling of the NADW. A sharp decrease in ventilation ages noticed during the B-A coincides with a rapid resumption of Atlantic overturning at the onset of the B-A warm period and an abrupt increase in well-ventilated, high-<sup>13</sup>C NADW flow into the Indian Ocean. Furthermore, changes in deep water ventilation are consistent with changes in atmospheric Δ<sup>14</sup>C which implicates changes in carbon exchange between the deep water and atmosphere. Our results thus demonstrate the Southern Ocean's role in ventilation changes of deep waters and hence its control over the exchange of <sup>14</sup>C between the ocean and atmosphere.

## CRedit authorship contribution statement

**Kumari Nisha:** Conceptualization, Data curation, Formal analysis, Methodology, Visualization, Writing- original draft; **Sushant Suresh Naik:** Conceptualization, Funding acquisition; Project administration; Resources; Supervision, Visualization, Writing- review & editing; **Pankaj Kumar:**

Formal analysis, Writing- review & editing; **Barnita Banerjee**: Formal analysis, Writing- review & editing; **Rama Murthy**: Formal analysis, Writing- review & editing.

### **Declaration of Competing Interest**

The authors declare that they have no known competing financial interests or personal relationships that could have appeared to influence the work reported in this paper. **Acknowledgements**

We are grateful to the Director of CSIR- National Institute of Oceanography, Goa, India for the permission to publish this research work. We thank the crew members of RV Sindhu Sadhana for their help and support during the sediment core collection. This core was obtained as a part of the MoES project 'Biogeochemical Processes and Paleoceanographic Studies of the Eastern Indian Ocean (MoES/36/OOIS/Extra/34/2013). We are thankful to the Inter-University Accelerator Centre (IUAC), Delhi, India for the AMS analyses. Yair Rosenthal and Vince Clementi of Rutgers are acknowledged for the age model calculations. KN is thankful to UGC for the research fellowship. This is NIO contribution No. XXXX.

### **Appendix A. Supplementary material**

Supplementary material related to this article can be found online at.....

### **References**

- Ahmad, S.M., Zheng, H., Raza, W., Zhou, B., Lone, M.A., Raza, T., Suseela, G., 2012. Glacial to Holocene changes in the surface and deep waters of the northeast Indian Ocean. *Mar. Geol.* 329-331, 16-23. <https://doi.org/10.1016/j.margeo.2012.10.002>.
- Anderson, R.F., Ali, S., Bradtmiller, L.I., Nielsen, S.H.H., Fleisher, M.Q., Anderson, B.E., Burckle, L.H., 2009. Wind-driven upwelling in the Southern Ocean and the deglacial rise in atmospheric CO<sub>2</sub>. *Science* 323(5920), 1443-1448. <https://doi.org/10.1126/science.1167441>.
- Bang, S., Huh, Y., Khim, B.K., Takata, H., Ikehara, M., Hyeong, K., Seo, I., Cho, H., 2021. Deep-Water Circulation over the Last Two Glacial Cycles Reconstructed from Authigenic Neodymium Isotopes in the Equatorial Indian Ocean (Core HI1808-GPC04). *Ocean Sci. J.* 1-10. <https://doi.org/10.1007/s12601-021-00046-8>.
- Barker, S., Knorr, G., Vautravers, M.J., Diz, P., Skinner, L.C., 2010. Extreme deepening of the Atlantic overturning circulation during deglaciation. *Nat. Geosci.* 3(8), 567-571. <https://doi.org/10.1038/ngeo921>.
- Bharti, N., Bhushan, R., Skinner, L., Muruganatham, M., Jena, P.S., Dabhi, A. and Shivam, A., 2022. Evidence of poorly ventilated deep Central Indian Ocean during the last glaciation. *Earth Planet. Sci. Lett.* 582, 117438. <https://doi.org/10.1016/j.epsl.2022.117438>.

- Böhm, E., Lippold, J., Gutjahr, M., Frank, M., Blaser, P., Antz, B., Fohlmeister, J., Frank, N., Andersen, M.B., Deininger, M., 2015. Strong and deep Atlantic meridional overturning circulation during the last glacial cycle. *Nature* 517(7532), 73-76. <https://doi.org/10.1038/nature14059>.
- Broecker, W., Mix, A., Andree, M., Oeschger, H., 1984. Radiocarbon measurements on coexisting benthic and planktic foraminifera shells: potential for reconstructing ocean ventilation times over the past 20 000 years. *Nucl. Instrum. Methods Phys. Res. Sect. B* 5(2), 331-339. [https://doi.org/10.1016/0168-583X\(84\)90538-X](https://doi.org/10.1016/0168-583X(84)90538-X).
- Broecker, W.S., Peng, T.H., Trumbore, S., Bonani, G., Wolfli, W., 1990. The distribution of radiocarbon in the glacial ocean. *Glob. Biogeochem. Cycles* 4(1), 103-117. <https://doi.org/10.1029/GB004i001p00103>.
- Broecker, W., Barker, S., 2007. A 190‰ drop in atmosphere's  $\Delta^{14}\text{C}$  during the “Mystery Interval”(17.5 to 14.5 kyr). *Earth Planet. Sci. Lett.* 256(1-2), 90-99. <https://doi.org/10.1016/j.epsl.2007.01.015>
- Bryan, S.P., Marchitto, T.M., Lehman, S.J., 2010. The release of  $^{14}\text{C}$ -depleted carbon from the deep ocean during the last deglaciation: Evidence from the Arabian Sea. *Earth Planet. Sci. Lett.*, 298(1-2), 244-254. <https://doi.org/10.1016/j.epsl.2010.08.025>.
- Burke, A., Robinson, L.F., 2012. The Southern Ocean’s role in carbon exchange during the last deglaciation. *Science* 335(6068), 557-561. <https://doi.org/10.1126/science.1208163>.
- Chandana, K.R., Bhushan, R. and Jull, A.J.T., 2017. Evidence of poor bottom water ventilation during LGM in the equatorial Indian Ocean. *Front. Earth Sci.* 5, 84. <https://doi.org/10.3389/feart.2017.00084>.
- Curry, W.B., Duplessy, J.C., Labeyrie, L.D., Shackleton, N.J., 1988. Changes in the distribution of  $\delta^{13}\text{C}$  of deep water  $\Sigma\text{CO}_2$  between the last glaciation and the Holocene. *Paleoceanography* 3(3), 317-341. <https://doi.org/10.1029/PA003i003p00317>.
- Duplessy, J.C., Shackleton, N.J., Matthews, R.K., Prell, W., Ruddiman, W.F., Caralp, M., Hendy, C.H., 1984.  $^{13}\text{C}$  record of benthic foraminifera in the last interglacial ocean: implications for the carbon cycle and the global deep water circulation. *Quat. Res.* 21(2), 225-243. [https://doi.org/10.1016/0033-5894\(84\)90099-1](https://doi.org/10.1016/0033-5894(84)90099-1).
- Dutta, K., Bhushan, R., Somayajulu, B., 2001.  $\Delta R$  correction values for the northern Indian Ocean. *Radiocarbon* 43(2A), 483-488. <https://doi.org/10.1017/S0033822200038376>.
- Elliot, M., Labeyrie, L., Duplessy, J.C., 2002. Changes in North Atlantic deep-water formation associated with the Dansgaard–Oeschger temperature oscillations (60–10 ka). *Quat. Sci. Rev.* 21(10), 1153-1165. [https://doi.org/10.1016/S0277-3791\(01\)00137-8](https://doi.org/10.1016/S0277-3791(01)00137-8).
- Freeman, E., Skinner, L.C., Tisserand, A., Dokken, T., Timmermann, A., Menviel, L., Friedrich, T., 2015. An Atlantic–Pacific ventilation seesaw across the last deglaciation. *Earth Planet. Sci. Lett.* 424, 237-244. <https://doi.org/10.1016/j.epsl.2015.05.032>.
- Galbraith, E.D., Jaccard, S.L., Pedersen, T.F., Sigman, D.M., Haug, G.H., Cook, M., Southon, J.R., Francois, R., 2007. Carbon dioxide release from the North Pacific abyss during the last deglaciation. *Nature* 449(7164), 890-893. <https://doi.org/10.1038/nature06227>.

- Galbraith, E.D., Jaccard, S.L., 2015. Deglacial weakening of the oceanic soft tissue pump: Global constraints from sedimentary nitrogen isotopes and oxygenation proxies. *Quat. Sci. Rev.* 109, 38–48. <https://doi.org/10.1016/j.quascirev.2014.11.012>.
- Galbraith, E.D., Kwon, E.Y., Bianchi, D., Hain, M.P., Sarmiento, J.L., 2015. The impact of atmospheric pCO<sub>2</sub> on carbon isotope ratios of the atmosphere and ocean. *Glob. Biogeochem. Cycles* 29(3), 307-324. <https://doi.org/10.1002/2014GB004929>.
- Gottschalk, J., Michel, E., Thöle, L.M., Studer, A.S., Hasenfratz, A.P., Schmid, N., Butzin, M., Mazaud, A., Martínez-García, A., Szidat, S. and Jaccard, S.L., 2020. Glacial heterogeneity in Southern Ocean carbon storage abated by fast South Indian deglacial carbon release. *Nat. Commun.* 11(1), pp.1-14.
- Hughen, K., Southon, J., Lehman, S., Bertrand, C., Turnbull, J., 2006. Marine-derived <sup>14</sup>C calibration and activity record for the past 50,000 years updated from the Cariaco Basin. *Quat. Sci. Rev.* 25(23-24), 3216-3227. <https://doi.org/10.1016/j.quascirev.2006.03.014>.
- Jung, S.J., Kroon, D., Ganssen, G., Peeters, F., Ganeshram, R., 2009. Enhanced Arabian Sea intermediate water flow during glacial North Atlantic cold phases. *Earth Planet. Sci. Lett.* 280(1-4), 220-228. <https://doi.org/10.1016/j.epsl.2009.01.037>.
- Kallel, N., Labeyrie, L.D., Juillet-Leclerc, A., Duplessy, J.C., 1988. A deep hydrological front between intermediate and deep-water masses in the glacial Indian Ocean. *Nature* 333(6174), 651-655. <https://doi.org/10.1038/333651a0>.
- Key, R.M., Olsen, A., van Heuven, S., Lauvset, S.K., Velo, A., Lin, X., Schirnick, C., Kozyr, A., Tanhua, T., Hoppema, M., Jutterström, S., 2015. Global ocean data analysis project, version 2 (GLODAPv2). Ornl/Cdiac-162, Ndp-093.
- Lathika, N., Rahaman, W., Tarique, M., Gandhi, N., Kumar, A., Thamban, M., 2021. Deep water circulation in the Arabian Sea during the last glacial cycle: Implications for paleo-redox condition, carbon sink and atmospheric CO<sub>2</sub> variability. *Quat. Sci. Rev.* 257, 106853. <https://doi.org/10.1016/j.quascirev.2021.106853>.
- Lauvset, S.K., Key, R.M., Olsen, A., Van Heuven, S., Velo, A., Lin, X., Schirnick, C., Kozyr, A., Tanhua, T., Hoppema, M., Jutterström, S., 2016. A new global interior ocean mapped climatology: The 1× 1 GLODAP version 2. *Earth Syst. Sci. Data* 8(2), pp.325-340.
- Lougheed, B.C., Obrochta, S.P., 2019. A rapid, deterministic age-depth modeling routine for geological sequences with inherent depth uncertainty. *Paleoceanogr. Paleoclimatol.* 34(1), 122-133. <https://doi.org/10.1029/2018PA003457>.
- Ma, R., Sépulcre, S., Licari, L., Bassinot, F., Liu, Z., Tisnérat-Laborde, N., Kallel, N., Yu, Z., Colin, C., 2019. Changes in intermediate circulation in the Bay of Bengal since the Last Glacial Maximum as inferred from benthic foraminifera assemblages and geochemical proxies. *Geochem. Geophys. Geosyst.* 20(3), 1592-1608. <https://doi.org/10.1029/2018GC008179>.
- Ma, R., Sepulcre, S., Bassinot, F., Haurine, F., Tisnérat-Laborde, N., Colin, C., 2020. North Indian Ocean circulation since the last deglaciation as inferred from new elemental ratio records for benthic foraminifera *Hoeglundina elegans*. *Paleoceanogr. Paleoclimatol.* 35(6), e2019PA003801. <https://doi.org/10.1029/2019PA003801>.

- Marchitto, T.M., Lehman, S.J., Ortiz, J.D., Flückiger, J., van Geen, A., 2007. Marine radiocarbon evidence for the mechanism of deglacial atmospheric CO<sub>2</sub> rise. *Science* 316(5830), 1456-1459. <https://doi.org/10.1126/science.1138679>.
- McManus, J.F., Francois, R., Gherardi, J.M., Keigwin, L.D., Brown-Leger, S., 2004. Collapse and rapid resumption of Atlantic meridional circulation linked to deglacial climate changes. *Nature* 428(6985), 834-837.
- Menviel, L., Yu, J., Joos, F., Mouchet, A., Meissner, K.J., England, M.H., 2017. Poorly ventilated deep ocean at the Last Glacial Maximum inferred from carbon isotopes: A data-model comparison study. *Paleoceanography*, 32(1), 2-17. <https://doi.org/10.1002/2016PA003024>.
- Monnin, E., Indermühle, A., Dällenbach, A., Flückiger, J., Stauffer, B., Stocker, T.F., Raynaud, D., Barnola, J.M., 2001. Atmospheric CO<sub>2</sub> concentrations over the last glacial termination. *Science* 291(5501), 112-114. <https://doi.org/10.1126/science.291.5501.112>.
- Naik, S.S., Naidu, P.D., Foster, G.L., Martínez-Botí, M.A., 2015. Tracing the strength of the southwest monsoon using boron isotopes in the eastern Arabian Sea. *Geophys. Res. Lett.* 42(5), 1450-1458. <https://doi.org/10.1002/2015GL063089>.
- Naik, S. S., Nisha, K., 2020. Increased ventilation of the northern Indian Ocean during the last deglaciation. *J. Geol. Soc. India* 96(2), 148-150. <https://doi.org/10.1007/s12594-020-1522-0>.
- Naqvi, W.A., Charles, C.D., Fairbanks, R.G., 1994. Carbon and oxygen isotopic records of benthic foraminifera from the Northeast Indian Ocean: implications on glacial-interglacial atmospheric CO<sub>2</sub> changes. *Earth Planet. Sci. Lett.* 121(1-2), 99-110. [https://doi.org/10.1016/0012-821X\(94\)90034-5](https://doi.org/10.1016/0012-821X(94)90034-5).
- Piotrowski, A.M., Banakar, V.K., Scrivner, A.E., Elderfield, H., Galy, A., Dennis, A., 2009. Indian Ocean circulation and productivity during the last glacial cycle. *Earth Planet. Sci. Lett.* 285(1-2), 179-189. <https://doi.org/10.1016/j.epsl.2009.06.007>.
- Primeau, F., 2005. Characterizing transport between the surface mixed layer and the ocean interior with a forward and adjoint global ocean transport model. *J. Phys. Oceanogr.* 35(4), 545-564. <https://doi.org/10.1175/JPO2699.1>.
- Rafter, P.A., Gray, W.R., Hines, S.K.V., Burke, A., Costa, K.M., Gottschalk, J., Hain, M.P., Rae, J.W.B., Southon, J.R., Walczak, M.H., Yu, J., Adkins, J.F., DeVries, T., 2022. Global reorganization of deep-sea circulation and carbon storage after the last ice age. *Sci. Adv.* 8(46). <https://doi.org/10.1126/sciadv.abq5434>.
- Raza, T., Ahmad, S.M., Sahoo, M., Banerjee, B., Bal, I., Dash, S., Suseela, G., Mukherjee, I., 2014. Hydrographic changes in the southern Bay of Bengal during the last ~ 65,000 y inferred from carbon and oxygen isotopes of foraminiferal fossil shells. *Quat. Int.* 333, 77-85. <https://doi.org/10.1016/j.quaint.2014.02.010>.
- Reimer, P.J., Austin, W.E., Bard, E., Bayliss, A., Blackwell, P.G., Ramsey, C.B., Butzin, M., Cheng, H., Edwards, R.L., Friedrich, M., Grootes, P.M., 2020. The IntCal20 Northern Hemisphere radiocarbon age calibration curve (0–55 cal kBP). *Radiocarbon* 62(4), 725-757. <https://doi.org/10.1017/RDC.2020.41>.



- Robinson, L.F., Adkins, J.F., Keigwin, L.D., Southon, J., Fernandez, D.P., Wang, S.L., Scheirer, D.S., 2005. Radiocarbon variability in the western North Atlantic during the last deglaciation. *Science* 310(5753), 1469-1473. <https://doi.org/10.1126/science.1114832>.
- Ronge, T.A., Tiedemann, R., Lamy, F., Köhler, P., Alloway, B.V., De Pol-Holz, R., Pahnke, K., Southon, J., Wacker, L., 2016. Radiocarbon constraints on the extent and evolution of the South Pacific glacial carbon pool. *Nat. Commun* 7(1), 1-12. <https://doi.org/10.1038/ncomms11487>.
- Ronge, T.A., Prange, M., Mollenhauer, G., Ellinghausen, M., Kuhn, G., Tiedemann, R., 2020. Radiocarbon evidence for the contribution of the Southern Indian Ocean to the evolution of atmospheric CO<sub>2</sub> over the last 32,000 years. *Paleoceanogr. Paleoclimatol.* 35(3), e2019PA003733. <https://doi.org/10.1029/2019PA003733>.
- Schlitzer, R., 2021. Ocean data view. <http://odv.awi.de>.
- Schott, F.A., McCreary Jr, J.P., 2001. The monsoon circulation of the Indian Ocean. *Prog.Oceanogr.* 51(1), 1-123. [https://doi.org/10.1016/S0079-6611\(01\)00083-0](https://doi.org/10.1016/S0079-6611(01)00083-0).
- Siani, G., Michel, E., De Pol-Holz, R., DeVries, T., Lamy, F., Carel, M., Isguder, G., Dewilde, F., Laurantou, A., 2013. Carbon isotope records reveal precise timing of enhanced Southern Ocean upwelling during the last deglaciation. *Nat. Commun.* 4(1), 1-9. <https://doi.org/10.1038/ncomms3758>.
- Sigman, D.M., Boyle, E.A., 2000. Glacial/interglacial variations in atmospheric carbon dioxide. *Nature* 407(6806), 859-869. <https://doi.org/10.1038/35038000>.
- Sikes, E.L., Cook, M.S., Guilderson, T.P., 2016. Reduced deep ocean ventilation in the Southern Pacific Ocean during the last glaciation persisted into the deglaciation. *Earth Planet. Sci. Lett.* 438, 130-138. <https://doi.org/10.1016/j.epsl.2015.12.039>.
- Singh, S.P., Singh, S.K., Goswami, V., Bhushan, R., Rai, V.K., 2012. Spatial distribution of dissolved neodymium and  $\epsilon$ Nd in the Bay of Bengal: Role of particulate matter and mixing of water masses. *Geochem. Cosmochim. Acta* 94, 38-56. <https://doi.org/10.1016/j.gca.2012.07.017>.
- Skinner, L.C., Shackleton, N.J., 2004. Rapid transient changes in northeast Atlantic deep water ventilation age across Termination I. *Paleoceanography* 19(2). <https://doi.org/10.1029/2003PA000983>.
- Skinner, L.C., Fallon, S., Waelbroeck, C., Michel, E., Barker, S., 2010. Ventilation of the deep Southern Ocean and deglacial CO<sub>2</sub> rise. *Science* 328(5982), 1147-1151. <https://doi.org/10.1126/science.1183627>.
- Skinner, L.C., Waelbroeck, C., Scrivner, A.E., Fallon, S.J., 2014. Radiocarbon evidence for alternating northern and southern sources of ventilation of the deep Atlantic carbon pool during the last deglaciation. *Proc. Nat. Acad. Sci USA* 111(15), 5480-5484. <https://doi.org/10.1073/pnas.1400668111>.
- Skinner, L., McCave, I.N., Carter, L., Fallon, S., Scrivner, A.E., Primeau, F., 2015. Reduced ventilation and enhanced magnitude of the deep Pacific carbon pool during the last glacial period. *Earth Planet. Sci. Lett.* 411, 45-52. <https://doi.org/10.1016/j.epsl.2014.11.024>.

- Skinner, L.C., Primeau, F., Freeman, E., de la Fuente, M., Goodwin, P.A., Gottschalk, J., Huang, E., McCave, I.N., Noble, T.L., Scrivner, A.E., 2017. Radiocarbon constraints on the glacial ocean circulation and its impact on atmospheric CO<sub>2</sub>. *Nat. Commun.* 8(1), 1-10. <https://doi.org/10.1038/ncomms16010>.
- Southon, J., Kashgarian, M., Fontugne, M., Metivier, B., Yim, W.W., 2002. Marine reservoir corrections for the Indian Ocean and Southeast Asia. *Radiocarbon* 44(1), 167-180. <https://doi.org/10.1017/S0033822200064778>.
- Stephens, B.B., Keeling, R.F., 2000. The influence of Antarctic sea ice on glacial–interglacial CO<sub>2</sub> variations. *Nature* 404(6774), 171-174. <https://doi.org/10.1038/35004556>.
- Toggweiler, J.R., Russell, J.L., Carson, S.R., 2006. Midlatitude westerlies, atmospheric CO<sub>2</sub>, and climate change during the ice ages. *Paleoceanography* 21(2). <https://doi.org/10.1029/2005PA001154>.
- Yadav, R., Naik, S.S., Narvekar, J., 2021. The equatorial Indian Ocean upper water-column structure influenced by cross-basinal water exchange over the last~ 40000 years. *Quat. Int.* <https://doi.org/10.1016/j.quaint.2021.04.002>.
- You, Y., 2000. Implications of the deep circulation and ventilation of the Indian Ocean on the renewal mechanism of North Atlantic Deep Water. *J. Geophys. Res. Oceans* 105(C10), 23895-23926. <https://doi.org/10.1029/2000JC900105>.
- Yu, Z., Colin, C., Ma, R., Meynadier, L., Wan, S., Wu, Q., Kallel, N., Sepulcre, S., Dapoigny, A., Bassinot, F., 2018. Antarctic Intermediate Water penetration into the Northern Indian Ocean during the last deglaciation. *Earth Planet. Sci. Lett.* 500, 67-75. <https://doi.org/10.1016/j.epsl.2018.08.006>.
- Zhang, H., Luo, Y., Yu, J., Zhang, L., Xiang, R., Yu, Z., Huang, H., 2022. Indian Ocean sedimentary calcium carbonate distribution and its implications for the glacial deep ocean circulation. *Quat. Sci. Rev.* 284, 107490. <https://doi.org/10.1016/j.quascirev.2022.107490>.

### Legends to figures:

Fig. 1. Core location (a) Map showing location of core SSD-044/GC-01 (CEIO; 4.99° N; 76.99° E; water depth = 3160 m) along with four other cores discussed in this study (RC27-23-Bryan et al., 2020; SS152/3828 and SS172/4040-Bharti et al., 2022; MD12-3396CQ-Gottschalk et al., 2020). The deep water circulation of the northern Indian Ocean is shown with blue arrows. (b) a cross-section of the Indian Ocean with core location showing modern  $\Delta^{14}\text{C}$  (GLODAPv2; Key et al., 2015; Lauvset et al., 2016). Both the plots were prepared using Ocean Data View (Schlitzer, 2021).

Fig. 2. (a) Measured radiocarbon ages of paired benthic and planktic foraminifera versus depth in the core SSD-044/GC-01.  $^{14}\text{C}$  age of benthic foraminifera (black circles),  $^{14}\text{C}$  age of planktic foraminifera (orange circles). (b) *Undatable* age-depth model for the core SSD-044/GC-01. The red line is median,

and the blue and black broken lines represent  $1\sigma$  and  $2\sigma$  confidence intervals, respectively. \*The model output of calibrated age (mean and median) at each cm interval along with the uncertainties and sediment accumulation rate (SAR) is provided in supplementary material. (c) Sediment accumulation rate (cm/kyr) plotted versus age in kyr BP.

Fig. 3. Graph showing changes in deep water circulation in the northern Indian Ocean during the last 25 kyr. (a) Ventilation ages (red square) which are plotted as benthic-planktic foraminifera radiocarbon age difference from core SSD-044/GC-01. The vertical error bars are the sum of the  $\pm$  error of the planktic and benthic foraminifera. The horizontal error bars signify the  $1\sigma$  depth errors. The red arrow indicates the modern ventilation age. (b) Calcium carbonate content in the sediment core SSD-044/GC-01. (c) Stable carbon isotopic data. The green arrow indicates the modern  $\delta^{13}\text{C}_{\text{DIC}}$ . (d) stable oxygen isotopic data of benthic foraminifera *Cibicidoides wuellerstorfi* from core SSD-044/GC-01. (e) Coarse fraction % ( $>63\ \mu\text{m}$ ) in core SSD-044/GC-01, and (f) sedimentary  $^{231}\text{Pa}/^{230}\text{Th}$  in core GGC5 (McManus et al., 2004). Climatic events such as Last Glacial Maxima (LGM), Henrich Stadial 1 (HS1), Bølling-Allerød (B-A) and Younger Dryas (YD) events are marked by dashed black lines and are shaded.

Fig. 4. Comparison of ventilation ages of the northern Indian Ocean to atmospheric  $\text{CO}_2$ , atmospheric  $\Delta^{14}\text{C}$ , and the Southern Ocean upwelling record during the last 25 kyr. (a) Atmospheric  $\text{CO}_2$  record (black circles; Monnin et al., 2001). (b) Atmospheric  $\Delta^{14}\text{C}$  is the IntCal20 calibration curve (grey line; Reimer et al., 2020). (c) The ventilation ages of the core SSD-044/GC-01 (red diamonds), core RC27-23 (orange circles; Bryan et al., 2020), core SS152/3828 (violet inverted triangles; Bharti et al., 2022), and core SS172/4040 (purple triangles; Bharti et al., 2022). These ventilation ages are plotted as benthic-planktic radiocarbon age differences. The vertical error bars are the sum of the  $\pm$  error of the planktic and benthic foraminifera. (d) Southern Ocean opal flux indicates upwelling in the Southern Ocean (Anderson et al., 2009). (e) Outgassing of  $\text{CO}_2$  from the surface water of the Arabian Sea (Naik et al., 2015). Climatic events Last Glacial Maxima (LGM), Henrich Stadial 1 (HS1), Bølling-Allerød (B-A), and Younger Dryas (YD) events are marked by dashed black lines and are shaded.

Fig. 1 (a)

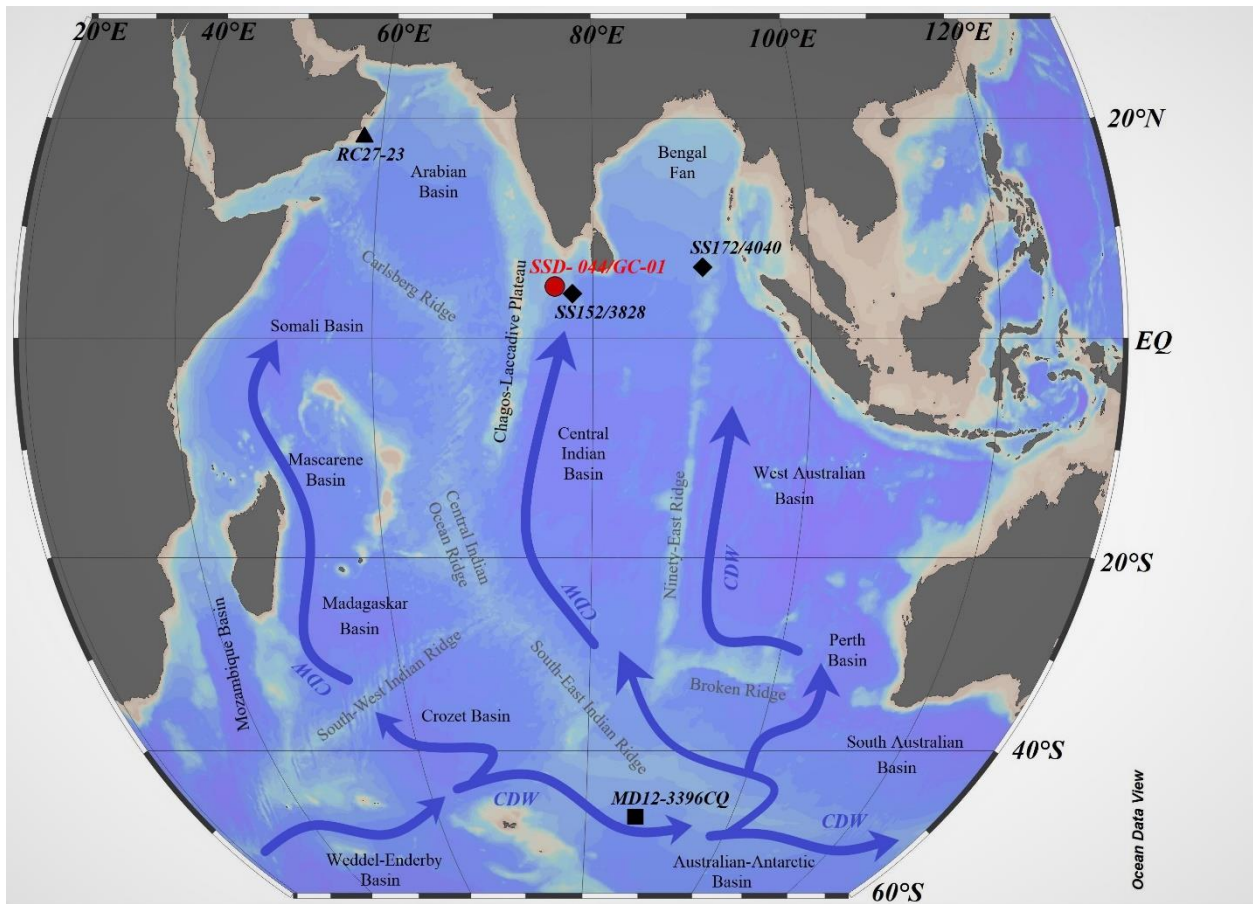


Fig. 1 (b)

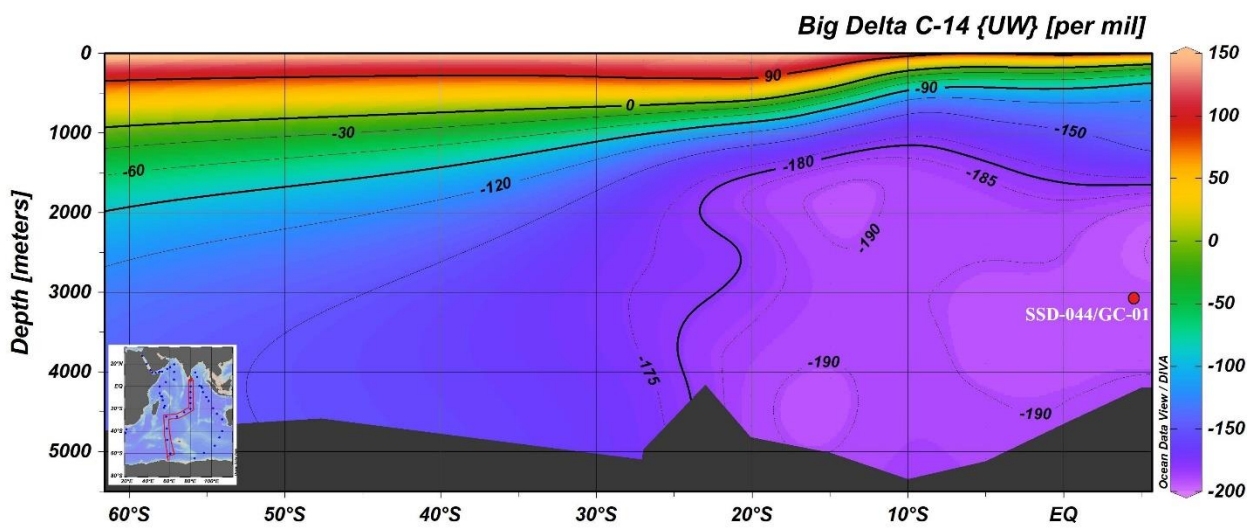


Fig. 2 (a)

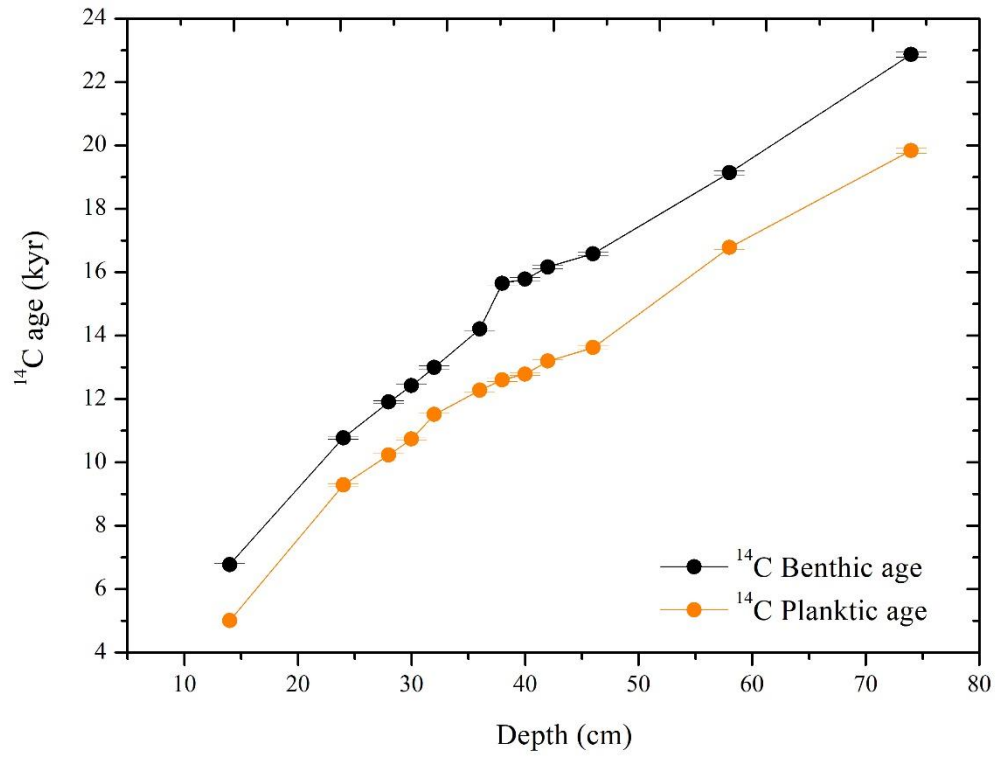


Fig. 2 (b)

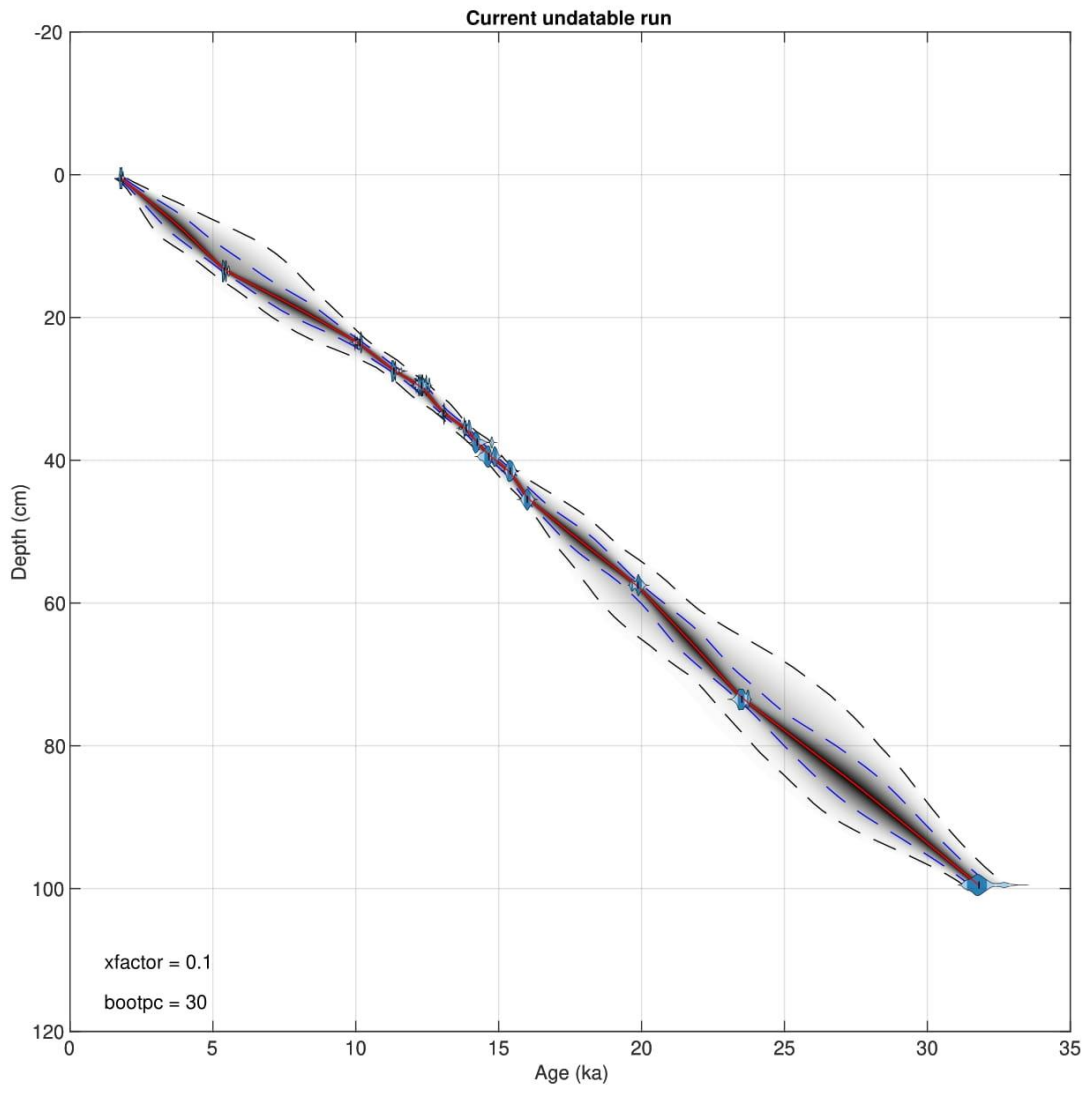


Fig. 2 (c)

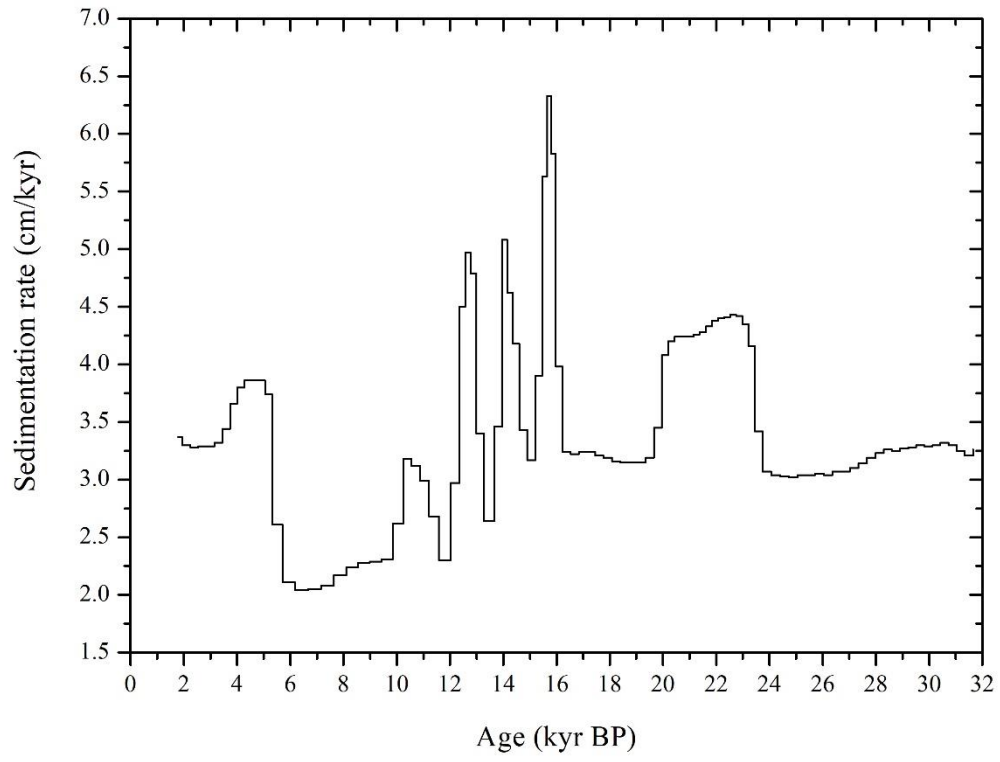


Fig. 3

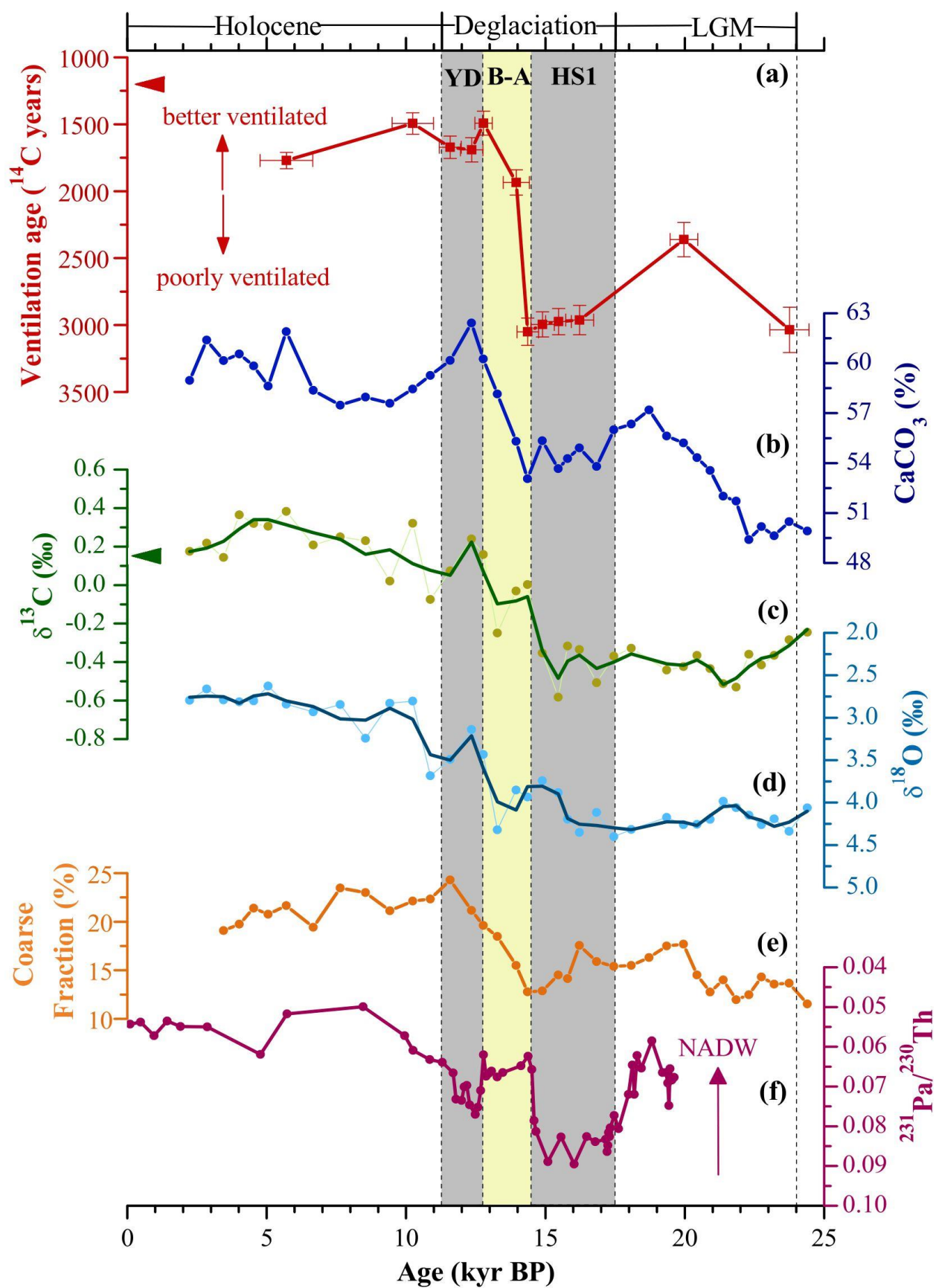




Fig. 4

